ACS APPLIED MATERIALS & INTERFACES

Research Article

www.acsami.org

Enhanced Durability of Polymer Electrolyte Membrane Fuel Cells by Functionalized 2D Boron Nitride Nanoflakes

Keun-Hwan Oh,[†,‡] Dongju Lee,[‡,§] Min-Ju Choo,[⊥] Kwang Hyun Park,[⊥] Seokwoo Jeon,[§] Soon Hyung Hong,*[,§] Jung-Ki Park,*[,⊥] and Jang Wook Choi*[,†,#]

[†]Graduate School of EEWS (Energy, Environment, Water, and Sustainability), [§]Department of Material Science and Engineering, Graphene Research Center (GRS), and KAIST Institute NanoCentury, [⊥]Department of Chemical and Biomolecular Engineering, and [#]Center for Nature-inspired Technology (CNiT), KAIST Institute NanoCentury, Korea Advanced Institute of Science and Technology, Daejeon 305-701, Korea

Supporting Information

ABSTRACT: We report boron nitride nanoflakes (BNNFs), for the first time, as a nanofiller for polymer electrolyte membranes in fuel cells. Utilizing the intrinsic mechanical strength of two-dimensional (2D) BN, addition of BNNFs even at a marginal content (0.3 wt %) significantly improves mechanical stability of the most representative hydrocarbon-type (HC-type) polymer electrolyte membrane, namely sulfonated poly(ether ether ketone) (sPEEK), during substantial water uptake through repeated wet/dry cycles. For facile processing with BNNFs that frequently suffer from poor dispersion in most organic solvents, we non-covalently functionalized BNNFs with 1-pyrenesulfonic acid (PSA). Besides good dispersion, PSA supports efficient proton transport through its sulfonic functional groups. Compared to bare sPEEK, the composite membrane containing BNNF nanofiller exhibited far improved long-term durability originating from enhanced dimensional stability and diminished chronic edge failure. This study suggests that introduction of properly functionalized 2D BNNFs is an effective strategy in making various HC-type membranes sustainable without sacrificing their original adventurous properties in polymer electrolyte membrane fuel cells.

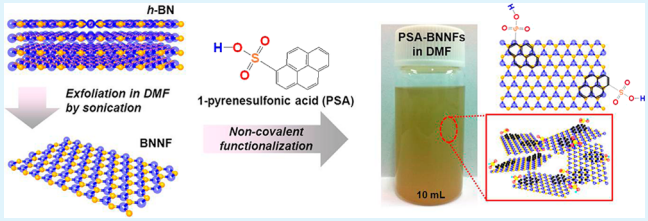

KEYWORDS: *boron nitride, composite membrane, durability, nanoflake, polymer electrolyte membrane fuel cell*

1. INTRODUCTION

Perfluorinated sulfonic acid (PFSA) polymers have been most widely adopted membrane materials for polymer electrolyte membrane fuel cells (PEMFCs). Despite their various advantageous properties,[1] most PFSA membranes suffer from critical drawbacks, such as high cost, environmentally hostile nature, limited temperature window for operation, and high fuel cross over. As an alternative approach to avoid these shortcomings, considerable efforts have been invested for development of hydrocarbon-type (HC-type) PEMs, and poly(arylene ether sulfone),[2] polybenzimidazole,[3] poly(arylene sulfide sulfone),[4] polyimide,[5] polyphenylene,[6] and poly(ether ether ketone) are good examples along this direction.[7]

A general design principle in synthesis of HC-type membranes is to conjugate a large number of sulfonic acid groups to the HC-polymer backbones because sulfonic acid groups can trigger hopping mechanism for proton conduction and can thus increase ion exchange capacities (IECs). However, the high IECs, in turn, result in significant water uptake, which leads to poor mechanical and dimensional stabilities. During repeated wet/dry cycles, those polymer membranes are subject to significant volume expansion/shrinkage,[8] whereas the electrodes on both sides tend to maintain the original dimensions. As a result, the initially well-bonded interfaces between the electrodes and membrane become impaired as the wet/dry cycle proceeds, leading to severe edge failures at the boundaries and consequently damaging the long-term cell durability.[9,10] Hence, avoiding swelling of HC-type PEMs and therefore addressing their long-term durability is now a very critical and challenging issue in the PEMFC community.

One of the most effective ways to resolve such unbalanced dimensional issue is to create reinforced composite membranes that contain additives with superior mechanical strengths.[11−14] However, the difficulty in use of those additives is that most conventional inorganic and polymeric additives simultaneously bring unwanted properties, such as phase separation with the mother electrolyte matrix, diminution of proton conductivity because of conduction channel blocking, and processing inconvenience from poor dispersion of additives.[13,15−18] In fact, it has been arduous to find any additives that could enhance the dimensional stability of the membranes without bypassing this trade-off situation.

On the other hand, few layered two-dimensional (2D) boron nitride (BN) nanosheets have been found to enhance the mechanical strengths of diverse composites when included even at minimal concentrations.[19−21] BN has additional advantages

Received: February 19, 2014
Accepted: April 7, 2014
Published: April 7, 2014

   dx.doi.org/10.1021/am5010317 | ACS Appl. Mater. Interfaces 2014, 6, 7751−7758

of low density, good thermal and chemical stability, electrically insulating property, and simple synthesis based on liquid exfoliation.[22−27] Nevertheless, BN has been considered as a nontrivial additive in actual processes because of its poor dispersion, low compatibility with polymer matrices, and natural aggregation by strong internal van der Waals interaction.[19,28] To overcome these processing drawbacks, BN nanosheets have been functionalized in both covalent and noncovalent approaches.[29,30] The covalent functionalization is based on chemical reactions with the functional groups on the BN surfaces. Thus, the surface functionalization could lose the intrinsic properties of BN sheets and also requires redundant synthetic steps.[20,31,32] By contrast, noncovalent functionalization could improve the solubility of BN sheets without sacrificing the original advantageous properties of BN. Polyaniline (PANI), DNA, and conjugated polymers[33,34] were used for such noncovalent functionalization. In spite of the increased solubility, the noncovalent functionalization known to date still has room for further improvement in expanding solvent pool and simplifying synthetic procedure. While searching for diverse approaches for noncovalent functionalization of BN, we were inspired by simple pyrene-based surface functionalization used for similar 2D layered graphene.[30,35] The planar structure of pyrene originating from four fused benzene rings accommodates well onto graphene sheets with similar planar morphology, particularly utilizing favorable $\pi-\pi$ interaction. After the pyrene-graphene assembly, the polar functional groups accompanied by pyrene endow the graphene sheets with increased solubility in various solvents and consequently processing capability. By expansion, in the current investigation, we increased the dispersion capability of similarly layered BN nanoflakes (BNNFs) by functionalizing nondestructively with 1-pyrenesulfonic acid (PSA), and incorporated them with one of the most well-known HC-type membranes, namely sulfonated poly(ether ether ketone) (sPEEK). The BNNF containing sPEEK composite membrane holds substantially enhanced mechanical strength even at a marginal BN content (0.3 wt %) and therefore addressed insufficient long-term durability of PEMFCs. Although BNNFs have been used in various research areas,[36−39] to the best of our survey, the current study is the first demonstration in the fuel cell area.

2. EXPERIMENTAL SECTION

Preparation of PSA-Functionalized BNNFs (PSA-BNNFs) and Their Characterizations. PSA-BNNFs were prepared through exfoliation of hexagonal BN (h-BN) microsized particles. In a typical experimental, BN powder (100 mg, KOJUNDO KOREA CO., LTD, used as received) was sonicated in 100 mL of *N*,*N*-dimethylformamide (DMF) containing 100 mg of 1-pyrenesulfonic acid (PSA, Aldrich) for 10 h. The dispersed BN solution was then centrifuged at 3000 rpm for 15 min to remove the aggregate and thick flakes. The supernatant was collected and washed several times with 500 mL of DMF to remove the unreacted PSA and then dried in a vacuum oven at 80 °C for 2 h. The yield of the final well-dispersed PSA-BNNFs (3 mg in 100 mL DMF) was about 3% with respect to the initial BN amount (100 mg).

The morphology of PSA-BNNFs was investigated using atomic force microscopy (AFM, Seiko Instrument Inc.) in tapping-mode under ambient condition. Transmission electron microscopy (TEM, JEOL JEM-2200FS) analyses were also conducted. The atomic force microscopy (AFM) and transmission electron microscopy (TEM) samples were prepared by drying a droplet of the PSA−BNNF suspension on a Si substrate and Lacey carbon grid, respectively. UV-Vis spectra were attained using an UV-3101PC spectrometer. FT-IR spectra were recorded using a Jasco FT/IR-4100 type-A spectrometer at ATM mode. X-ray photoelectron spectroscopy (XPS) experiments were performed using a Sigma Probe (Thermo VG Scientific, AlKα). For thermogravimetric analysis (TGA) measurements, a TGA 92-18 device (Setaram) was used in the temperature from 20 to 900 °C at a heating rate of 10 °C min^{-1} in air. To investigate the hydrophilic character of PSA-BNNFs, we measured water contact angles by using a contact angle analyzer (Phoenix 300 Plus, SEO Co.)

Preparation of Bare and Composite Membrane and Its Characterizations. sPEEK was prepared by sulfonation of poly(ether ether ketone) (Aldrich) according to a procedure reported elsewhere.[40] The 1 g of sPEEK was dissolved in the 9 g (9.45 mL) of PSA-BNNF suspension in DMF. The entire 10 g of the homogeneous mixture of PSA-BNNFs and sPEEK was directly cast onto a clean glass plate (300 mm × 200 mm) by using a 600 μm thick doctor blade at a constant speed of 3 cm s^{-1}, and dried at 60 °C for 24 h and subsequently dried again under vacuum at 120 °C for the following 24 h. The membrane was peeled off from the glass plate by submersing it in deionized water. The thickness of all the membranes prepared in this study was about 40 μm.

Water uptakes and dimensional changes were measured by the differences in weight and dimensions of the membranes before and after a wet treatment. For preparation of the wet membrane, the membranes were soaked into deionized water at 80 °C for 1 h and were then wiped out and the weight, length, and thickness were measured immediately. The dry membrane was obtained after vacuum drying at 60 °C for 24 h. Water uptake and dimensional change Δl (or Δt) of the membranes were calculated based on the following equations

$$\text{water uptake (\%)} = \frac{W_{\text{wet}} - W_{\text{dry}}}{W_{\text{dry}}} \times 100$$

$$\Delta l \text{ (or } \Delta t) = \frac{l_{\text{wet}} - l_{\text{dry}}}{l_{\text{dry}}} \left(\text{or } \frac{t_{\text{wet}} - t_{\text{dry}}}{t_{\text{dry}}} \right) \times 100$$

where W_{wet}, l_{wet}, and t_{wet} are the weight, length, and thickness of the wet membrane, respectively. W_{dry}, l_{dry}, and t_{dry} are defined similarly for the dry membrane.

The IEC of the membrane was measured by the classical titration method. The membrane was soaked in saturated NaCl aqueous solution with excessive volume for 12 h. The solution was then titrated toward an end point of pH 7 with a standard 0.01 M NaOH aqueous solution based on the following equation

$$\text{IEC (mequiv g}^{-1}) = \frac{VM}{m_{\text{dry}}}$$

, where V, M, and m_{dry} are the volume of the titrant, the molar concentration of the titrant, and the mass of the sample, respectively.

The ionic conductivities of the bare and composite membranes were determined by using AC impedance spectroscopy measurements (1400 FRA and 1470E, Solartron) over a frequency range from 1 × 10^5 to 0.1 Hz.

Stress-strain curves of the bare and composite membranes were attained by using a universal testing machine (Instron 5583) at room temperature with a strain rate of 20 mm min^{-1}. To investigate the water state of membrane, we conducted thermal analyses by using differential scanning calorimetry (DSC, DuPont TA 2000) calibrated with indium was used with dried samples. Each sample was first cooled from 25 to −50 °C and then heated at a rate of 5 °C min^{-1} to 150 °C.

Fabrication of Membrane Electrode Assemblies (MEAs) and Electrochemical Characterization. MEAs were fabricated by transfer of the anode and the cathode catalyst layers (CLs) on Kapton film to each side of the membrane at a pressure of 1500 psi and at 130 °C for 3 min. After cooling to room temperature, the Kapton films were peeled off from the laminates.[40] The catalyst loading and the catalyst transference ratio were obtained by measuring the CL mass difference before and after the hot pressing. Pt loading level of all the CLs was carefully controlled to be within 0.25 ± 0.02 mg cm^{-2} and the sizes of the CLs were 5 × 5 cm^2. A cell was

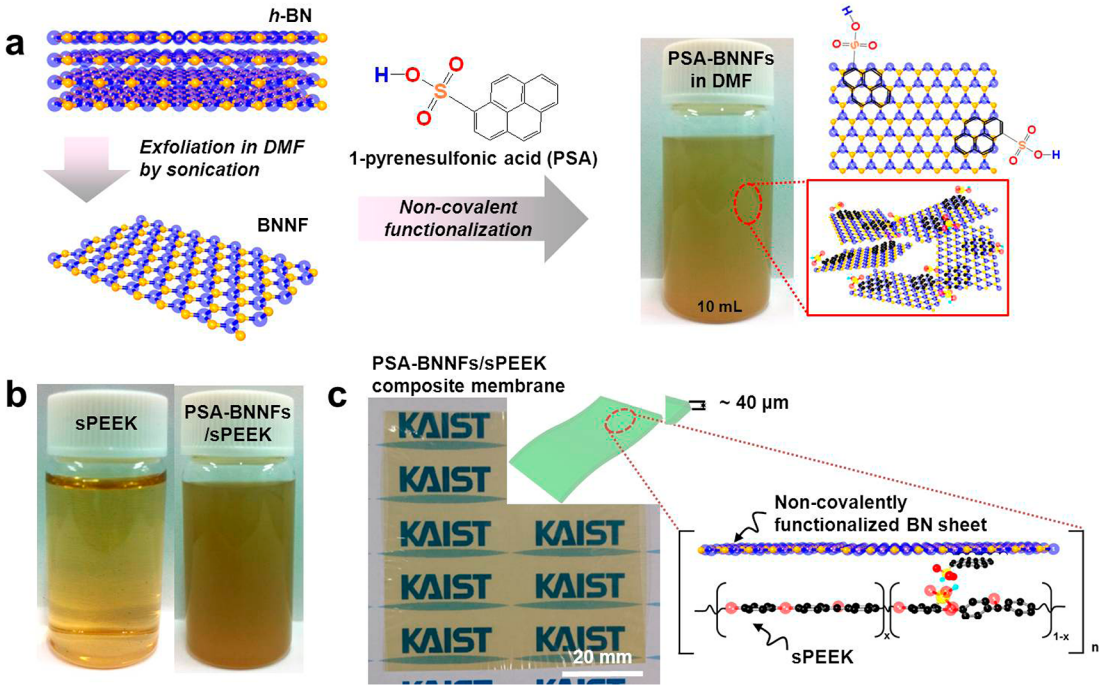

Figure 1. Schematic diagram indicating the overall procedure for preparation of PSA-BNNFs and PSA-BNNFs/sPEEK composite membrane. (a) Schematic illustration of exfoliated BNNFs from hexagonal BN by sonication in DMF containing 1-PSA alongside an actual photograph of highly dispersed PSA-BNNFs solution. (b) Photograph of bare sPEEK and PSA-BNNFs/sPEEK solutions. (c) Photograph of PSA-BNNFs/sPEEK composite membrane after solution casting and drying together with a graphical description of the interaction between PSA-BNNF and sPEEK.

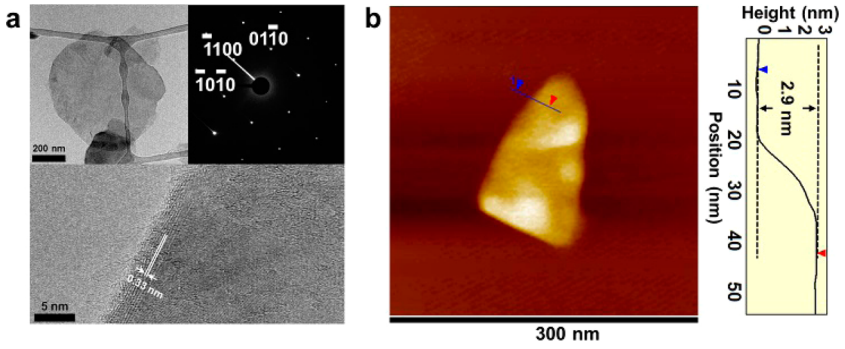

Figure 2. Morphology of PSA-BNNFs. (a) Low- (top left) and high- magnification (bottom) TEM images and corresponding SAED pattern (top right) of PSA-BNNFs. (b) An AFM topography image (dimension: 300 nm × 300 nm) of PSA-BNNF on the SI substrate. (Right) The height profile along the black line shown in the AFM image.

completed by assembling the MEA, a pair of gas diffusion media (35BC, SGL), a pair of Teflon gaskets, and a pair of graphite blocks with a triple serpentine flow field for reactants. The flow fields for the anode and cathode reactants were symmetric.

The IV polarization curves of each single cell were obtained at a fuel cell test station (CNL, Korea). The anode was fed with humidified hydrogen gas (RH 100%) at a flow rate of 500 $cm^3\ s^{-1}$ and the cathode was fed with humidified air (RH 100%) at a flow rate of 1500 $cm^3\ s^{-1}$, which correspond to the stoichiometry of H_2/air = 14.3/18.0 at 0.2 A cm^{-2}. The actual IV polarization curve of each cell was obtained at 80 °C without back pressure after a 3 day fuel cell operation to saturate the cell performance under fuel supply. Electrochemical impedance spectroscopic measurements were performed using an AC impedance analyzer (1400 FRA and 1470E, Solartron) in which the AC amplitude was 10 mV, and the frequency range was from 1×10^5 to 0.1 Hz.

Wet/Dry Cycle Tests of MEAs. After an initial evaluation of IV polarization curve, wet/dry cycle tests were conducted to examine the effect of the PSA-BNNFs nanofiller on the cell performance under repeated hydration and dehydration cycles. For this experiment, nonhumidified and fully humidified nitrogen gas was alternately fed every 2 min at a flow rate of 1000 $cm^3\ s^{-1}$. Such humidification was controlled by (dis)connection to a humidifier. During these repeated cycles, the curren−-voltage curve and open circuit voltage (OCV) were monitored every 50 humidity cycles.

3. RESULTS AND DISCUSSION

Figure 1 schematically illustrates the overall procedure of PSA functionalization onto the BNNFs and their inclusion into sPEEK composite electrolyte together with a digital photograph at each stage. BNNFs were first exfoliated from BN powder and subsequently functionalized with PSA molecules by sonication in *N*,*N*-dimethylformamide (DMF) containing PSA (0.3 wt %, Figure 1a). During this process, pyrene groups of PSA molecules bind onto BNNF surfaces by favorable $\pi-\pi$ interaction without structural destruction, and these $\pi-\pi$ interactions originate from electronic attraction between the π-electron-deficient BNNFs and the π-electron-rich pyrene groups of PSA molecules. PSA-BNNFs were well-dispersed in

dx.doi.org/10.1021/am5010317 | ACS Appl. Mater. Interfaces 2014, 6, 7751−7758

DMF because of the polar characteristic of the sulfonic groups in PSA (Figure 1b). The PSA-BNNF preserved the good dispersion even after mixing with sPEEK polymer electrolyte (Figure 1b). This mixture was then cast to form films and subsequently dried to produce the final PSA-BNNFs/sPEEK composite membranes with thicknesses near 40 μm (Figure 1c). The good dispersion of the mixture must be associated with the common amphiphilic nature of both components.

BNNFs maintained their original 2D morphology even after the PSA functionalization as shown in Figure 2. The planar geometry of BNNFs was observed from low-magnification TEM characterization, and the hexagonal honeycomb-like atomic configuration of h-BN was confirmed by selected area electron diffraction pattern (SAED) that exhibited spots with six-fold symmetry when the beam orientation was aligned along the [0001] direction. Also, the lattice distance of the folded edge was observed to be ~0.33 nm, which is consistent with the layer-to-layer distance of h-BN across the 2D stacking orientation (Figure 2a).[19] The thickness of a single PSA-BNNF estimated by a height profile of AFM scanning (Figure 2b) was 2.7−3.1 nm, corresponding to 8−10 BN layers.

The surface functionalization of BNNFs was analyzed by spectroscopic characterizations and TGA. Figure 3a comparatively displays FT-IR spectra of PSA, BNNFs, and PSA-BNNFs. BNNFs exhibited strong absorption peaks at 1348 and 782 cm^{-1} assigned to the B−N stretching (in-plane ring vibration) and B−N bending (out of plane vibration), respectively.[22] On the other hand, the spectrum of PSA showed peaks at 1180 and 1048 cm^{-1}, corresponding to the stretching vibration of sulfonic acid groups of PSA. After the noncovalent interaction, PSA-BNNFs showed combined peaks from both PSA and BNNFs but with some peak locations shifted, which is ascribed to the π-electron state changes of both pyrene groups of PSA and BN after their $\pi-\pi$ interaction. This peak shift is commensurate with previous studies.[41−44] The UV−Vis spectra of the same three samples consistently support the $\pi-\pi$ electron interaction between both components (see Figure S1 in the Supporting Information).

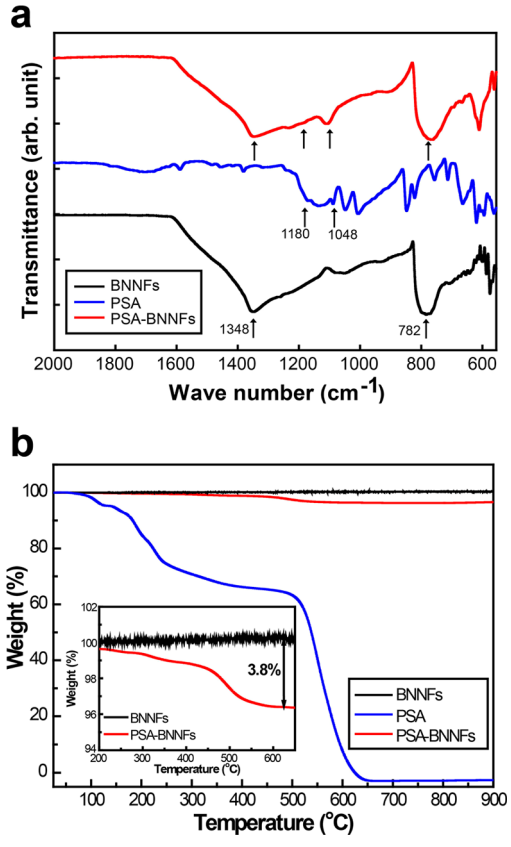

Figure 3. (a) FT-IR spectra of BNNFs, PSA, and PSA-BNNFs. (b) TGA profiles of the same three samples in the temperature range from RT to 900 °C at a heating rate of 10 °C min^{-1} in air. (Inset) The same data but magnified in the smaller weight range.

The TGA results (Figure 3b) provide further information on PSA-BNNFs. While BNNFs exhibited excellent thermal stability up to 900 °C, PSA began to show a weight loss in the temperature range of 130−450 °C originating from decomposition of the sulfonic acid group and another weight loss in the temperature range of 450−650 °C originating from decomposition of the pyrene group in PSA. The TGA curve of PSA-BNNFs, however, followed a similar profile to that of BNNFs. From a larger magnification (Figure 3b inset), the similar stepwise loss behavior to that of PSA was observed with an overall weight loss reaching ~3.8 wt %, reflecting the content of PSA involving the surface functionalization. In addition, XPS data support the PSA functionalization onto BNNFs (see Figure S2 in the Supporting Information) on the basis of the presence of the relevant elemental bands (C 1s, B 1s, N 1s, O 1s, and S 2p). It is particularly noticeable that the C 1s peak can be deconvoluted into two sub-peaks corresponding to the carbons from the sp^2 pyrene moieties (284.6 eV) and $-C-SO_3H$ functional groups (286.6 eV). Water contact angle of PSA-BNNFs thin film was also measured to see the effect of the PSA functionalization on the surface property of BNNFs. As shown in Figure S3 in the Supporting Information, the contact angles with and without the PSA functionalization were 66 and 90°, respectively, indicating the enhanced hydrophilic nature of BN by the PSA functionalization.

Prior to electrochemical testing, we investigated various physical properties for PSA-BNNFs/sPEEK composites with different PSA-BNNFs contents:

(1) In the mechanical strength perspective (Figure 4a), the composite membrane with 0.3 wt % PSA-BNNFs showed the highest ultimate tensile strength of 47.2 MPa, which corresponds to 41% increase compared to that of bare sPEEK. At this PSA-BNNF content, the strength of the composite becomes maximized utilizing the intrinsic mechanical strength of BN and good dispersion of its flakes.[45−47] In particular, the good dispersion of PSA-BNNFs must be critical in the enhanced strength and cell performance because the BNNF-sPEEK contacts through large surface areas allow for transferring the intrinsically superior mechanical strength of BN to the composite efficiently[48,49] while the decent electrochemical properties of sPEEK is impaired only to a minimal degree. Once the PSA-BNNFs content goes beyond 0.3 wt %, the tensile strength weakens because the interaction between both components decreases due to aggregation of PSA-BNNFs.

(2) Interestingly, the IEC and proton conductivity also exhibited the highest values at 0.3 wt % PSA-BNNFs (Figures 4b and c). The IEC behavior can be interpreted again by the optimized dispersion of PSA-BNNFs that allows the largest number of sulfonic groups available for the titration at this PSA-BNNFs content. Up to 0.3 wt %, addition of PSA-BNNFs contributes to increasing the total number of sulfonic group, but its effect drops beyond 0.3 wt % once again due to aggregation of PSA-BNNFs. Similarly, below 0.3 wt %, the

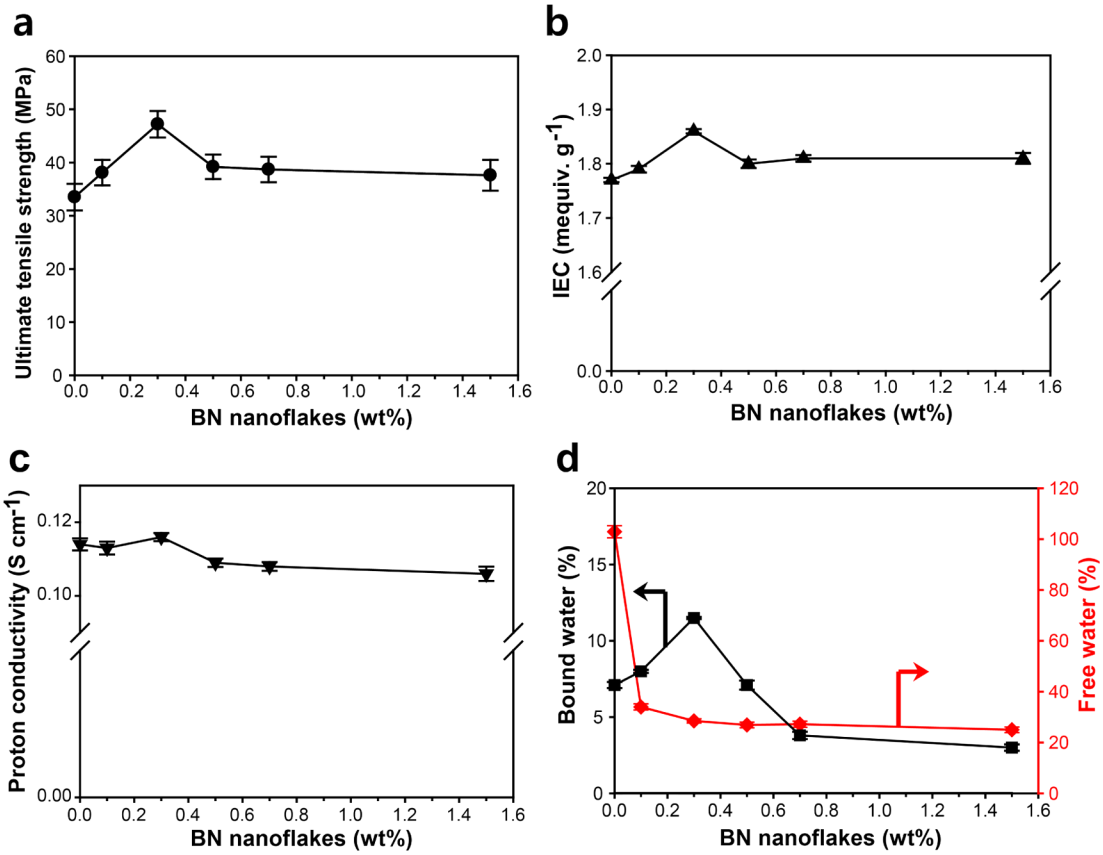

Figure 4. Various physical properties of the composite membranes with various PSA-BNNFs contents. (a) Ultimate tensile strength, (b) ion exchange capacity, (c) proton conductivity, and (d) bound and free water uptake.

proton conductivity remained at the initial level by dominant nature of sPEEK but increased by addition of PSA-BNNFs up to 0.3 wt %. After this point, however, the conductivity went down due to conducting channel blocking from aggregated PSA-BNNFs.

(3) The aggregate formation beyond 0.3 wt % was visualized by SEM characterization (see Figure S4 in the Supporting Information). Although all of the surface images showed similar smooth and homogeneous morphologies, the cross-sectional SEM images showed the large sizes of PSA-BNNFs aggregates for the PSA-BNNFs contents above 0.5 wt %.

(4) The proton transport of the composite membrane can also be correlated with the content of so-called bound water. The state of water in typical PEMs is classified into two kinds: free water and bound water. Between these two, the bound water plays a central role in the proton transport through PEMs[50,51] because the bound water facilitates proton transfer through interaction with the sulfonic acid groups in ionomers, whereas the free water that is not bound to the polymer chains and thus behaves like bulk water does not serve such function.[50] The bound water forms hydrogen bonding with sulfonic groups, and proton can diffuse through the bound water by forming hydronium ions during its hopping. As in the aforementioned points 1−3, at 0.3 wt % PSA-BNNFs, the bound water exhibited the highest value (Figure 4d), thus supporting the highest proton conductivity at this content. Also, water uptake (see Figure S5 in the Supporting Information) follows the same trend as that of the free water. Consistent with previous reports,[52] the increased amount of nanofiller (BNNFs in our case) decreased the water uptake because of reduction in free volume as well as its occupation near ionic clusters. The decreased water uptake with the PSA-BNNFs content decreased the dimensional change of the composite membrane (see Table S1 in the Supporting Information). Overall, 0.3 wt % is therefore the golden spot in both dispersion of BNNFs and bound water content.

To evaluate the PSA-BNNFs effect on the cell performance, especially focusing on long-term durability, we carried out OCV and galvanostatic polarization measurements over repeated wet/dry cycles by engaging the U.S. Department of Energy (DOE) protocol (see Figure S6 in the Supporting Information). Figure 5a−c shows the galvanostatic polarization curves of the composite membranes with 0.3, 0, and 0.7 wt % of PSA-BNNFs, respectively, before and after a large number of wet/dry cycles. The 0.3 wt % case exhibited only moderate galvanostatic curve decay after 950 cycles (Figure 5a), whereas the 0 wt % case showed much more pronounced decay even after 500 cycles (Figure 5b). In the case of 0.7 wt % (Figure 5c), the polarization curve started at lower voltages over the same range of the current density even in the initial cycle and was also worse at maintaining the voltages after cycling. The current density change at 0.6 V represents the observed trend over this series of samples (Figure 5a−c, insets): (i) 0.3 wt %, 376 → 338 mA cm^{-2} after 950 cycles; (ii) 0 wt %, 360 → 0 mA cm^{-2} after 500 cycles; (iii) 0.7 wt %, 314 → 0 mA cm^{-2} after 650 cycles.

Furthermore, the OCV results (Figure 5d) measured during the same repeated wet/dry cycles also showed the consistent trend among the samples. The OCVs of 0.3, 0, and 0.7 wt % samples showed distinctive performance, such as 0.95 → 0.88 V

dx.doi.org/10.1021/am5010317 | ACS Appl. Mater. Interfaces 2014, 6, 7751−7758

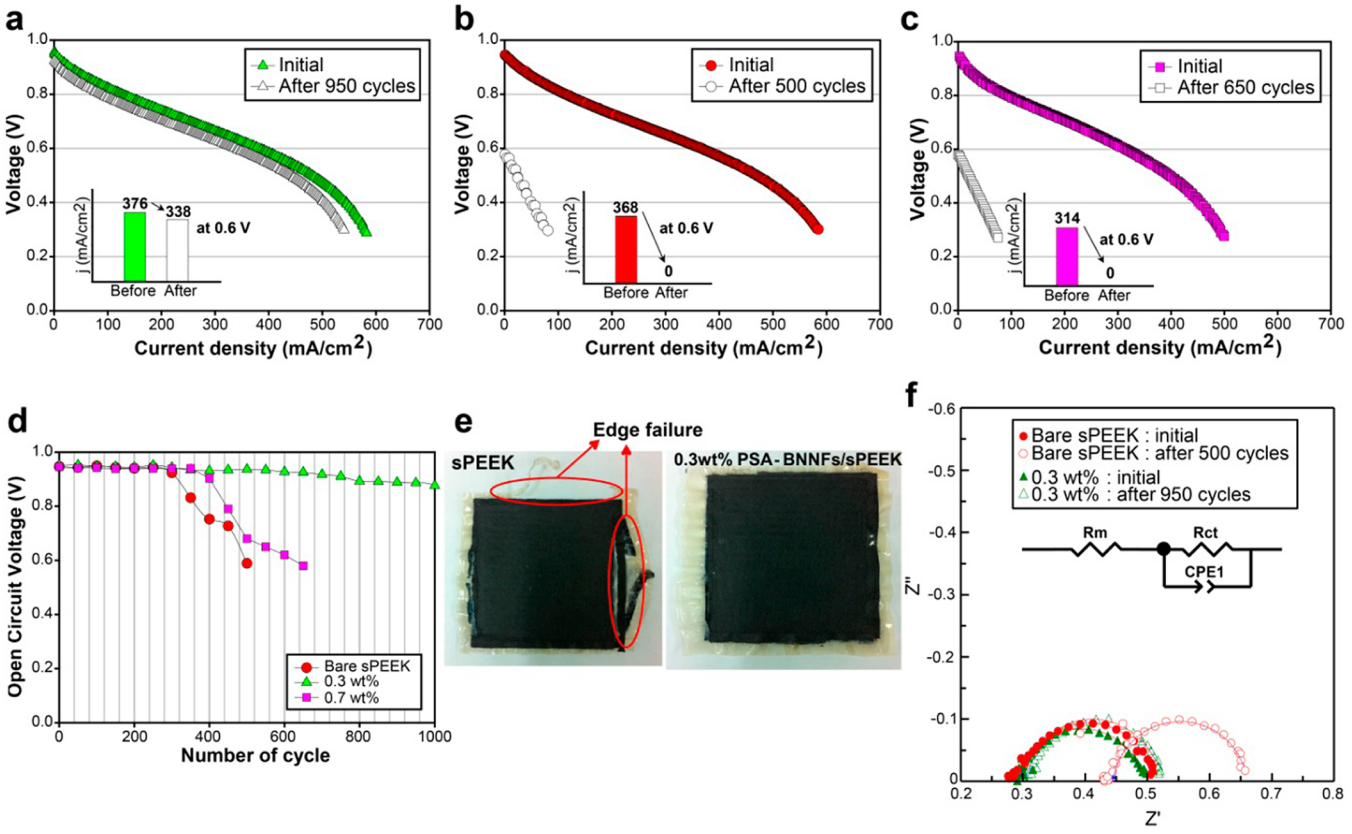

Figure 5. Electrochemical characterization of sPEEK-based PEMFCs incorporating various PSA-BNNF contents. Galvanostatic polarization curves of the cells with (a) 0.3, (b) 0, and (c) 0.7 wt % PSA-BNNFs before and after designated numbers of wet/dry cycles. Insets are the current density changes at 0.6 V. (d) OCV changes during wet/dry cycles for the 0, 0.3, and 0.7 wt % PSA-BNNF cases. (e) Optical images of the bare sPEEK and 0.3 wt % PSA-BNNFs/sPEEK composite membranes after 500 and 950 wet/dry cycles. The bare sPEEK membrane (left) shows typical edge failure, which is in sharp contrast against the composite membrane (right). (f) Nyquist plots for the 0 and 0.3 wt % case before and after the wet/dry cycles denoted in the figure legend.

after 950 cycles, 0.95 → 0.58 V after 500 cycles, and 0.94 → 0.59 V after 650 cycles, corresponding to 93%, 61%, and 63% OCV retentions, respectively. The superior retentions of the 0.3 wt % case in both galvanostatic polarization curve and OCV are attributed to the diminished local damages such as edge failure at the active−inactive boundaries (Pt catalyst was loaded only in the middle active region) and membrane creeping during repeated swelling/shrinking processes.[53] In our particular cases, because severe membrane creep was not observed as seen in Figure 5e, the degradation by edge failure appears to be more critical.

To further confirm the improvement of the long-term durability, we recorded impedance spectra at 0.6 V for the 0.3 and 0 wt % cases (Figure 5f). In PEMFCs, the bulk resistance (R_m) is usually dictated by proton conductivity through the membrane and/or at electrode-electrolyte interfaces, and is determined by the intercept at the real axis of the Nyquist plot.[54] The improved durability by introduction of the optimal amount of PSA-BNNFs was reconfirmed by R_m. Although both types of membranes showed similar R_m (~0.29 Ω cm^2) before cycling, the 0.3 wt % composite membrane was substantially better at maintaining the original R_m compared to the 0 wt % counterpart after 950 wet/dry cycles (0.299 vs. 0.445 Ω cm^2), which is again commensurate with the galvanostatic and OCV measurements and verifies the crucial role of PSA-BNNFs. We also determined the CL resistance (R_{cl}) and charge-transfer resistance (R_{ct}) from the impedance data (see Table S2 in the Supporting Information) and confirmed that the performance fading is mainly from membrane degradation, not from catalyst degradation. See the Supporting Information for details.

4. CONCLUSION

In the present study, the markedly improved long-term durability of PEMFC was achieved by incorporating 2D BNNFs non-covalently functionalized with PSA into the sPEEK PEM. Even with the marginal content of PSA-BNNFs, the intrinsic mechanical strength of BN makes the composite membrane more resistant against the chronic edge failure associated with the volume expansion/shrinkage of the membrane over a large number of wet/dry cycles. The successful demonstration of BN incorporation in the current investigation suggests that properly functionalized BNNFs could be used for a variety of other applications where polymer suffers from insufficient mechanical stability without sacrificing its original properties.

■ ASSOCIATED CONTENT

Supporting Information

UV−vis/XPS spectra of PSA-BNNFs, SEM, and water uptake of the composite membranes, wet/dry cycling protocol for long-term operation, optical images of the composite membranes after cycles, dimensional/resistance changes of the composite membranes. This material is available free of charge via the Internet at http://pubs.acs.org.

AUTHOR INFORMATION

Corresponding Authors

*E-mail: shhong@kaist.ac.kr.
*E-mail: jungpark@kaist.ac.kr.
*E-mail: jangwookchoi@kaist.ac.kr.

Author Contributions

‡Authors K.-H.O. and D.L. contributed equally. The manuscript was written through contributions of all authors. All authors have given approval to the final version of the manuscript.

Notes

The authors declare no competing financial interest.

ACKNOWLEDGMENTS

This work was supported by New & Renewable Energy R&D program (20113020030020) under the Ministry of Knowledge Economy, Republic of Korea. J.W.C. acknowledges financial support by the National Research Foundation of Korea (NRF) grant funded by the Korea government (MEST) (NRF-2012-R1A2A1A01011970). S.J. and S.H.H. acknowledge financial support by the Center for Advanced Soft Electronics under the Global Frontier Research Program of the Ministry of Science, ICT & Future Planning, Korea (2013M3A6A5073173).

REFERENCES

(1) Mauritz, K. A.; Moore, R. B. State of Understanding of Nafion. *Chem. Rev.* **2004**, *104*, 4535−4586.

(2) Wang, F.; Hickner, M.; Kim, Y. S.; Zawodzinski, T. A.; McGrath, J. E. Direct Polymerization of Sulfonated Poly(arylene ether sulfone) Random (statistical) Copolymers: Candidates for New Proton Exchange Membranes. *J. Membr. Sci.* **2002**, *197*, 231−242.

(3) Xiao, L.; Zhang, H.; Scanlon, E.; Ramanathan, L. S.; Choe, E.-W.; Rogers, D.; Apple, T.; Benicewicz, B. C. High-Temperature Polybenzimidazole Fuel Cell Membranes via a Sol−Gel Process. *Chem. Mater.* **2005**, *17*, 5328−5333.

(4) Wiles, K. B.; Wang, F.; McGrath, J. E. Directly Copolymerized Poly(arylene sulfide sulfone) Disulfonated Copolymers for PEM-based Fuel Cell Systems. I. Synthesis and Characterization. *J. Polym. Sci., Part A: Polym. Chem.* **2005**, *43*, 2964−2976.

(5) Fang, J.; Guo, X.; Harada, S.; Watari, T.; Tanaka, K.; Kita, H.; Okamoto, K.-i. Novel Sulfonated Polyimides as Polyelectrolytes for Fuel Cell Application. 1. Synthesis, Proton Conductivity, and Water Stability of Polyimides from 4,4′-Diaminodiphenyl Ether-2,2′-disulfonic Acid. *Macromolecules* **2002**, *35*, 9022−9028.

(6) He, L.; Fujimoto, C. H.; Cornelius, C. J.; Perahia, D. From Solutions to Membranes: Structure Studies of Sulfonated Polyphenylene Ionomers. *Macromolecules* **2009**, *42*, 7084−7090.

(7) Xing, P.; Robertson, G. P.; Guiver, M. D.; Mikhailenko, S. D.; Wang, K.; Kaliaguine, S. Synthesis and Characterization of Sulfonated Poly(ether ether ketone) for Proton Exchange Membranes. *J. Membr. Sci.* **2004**, *229*, 95−106.

(8) Sankir, M.; Kim, Y. S.; Pivovar, B. S.; McGrath, J. E. Proton Exchange Membrane for DMFC and H_2/air Fuel Cells: Synthesis and Characterization of Partially Fluorinated Disulfonated Poly(arylene ether benzonitrile) Copolymers. *J. Membr. Sci.* **2007**, *299*, 8−18.

(9) Lin, C. W.; Huang, Y. F.; Kannan, A. M. Semi-Interpenetrating Network based on Cross-linked Poly(vinyl alcohol) and Poly(styrene sulfonic acid-co-maleic anhydride) as Proton Exchange Fuel Cell Membranes. *J. Power Sources* **2007**, *164*, 449−456.

(10) Oh, K.-H.; Choo, M.-J.; Lee, H.; Park, K. H.; Park, J.-K.; Choi, J. W. Mussel-Inspired Polydopamine-Treated Composite Electrolytes for Long-Term Operations of Polymer Electrolyte Membrane Fuel Cells. *J. Mater. Chem. A* **2013**, *1*, 14484−14490.

(11) Chang, J.-H.; Park, J. H.; Park, G.-G.; Kim, C.-S.; Park, O. O. Proton-Conducting Composite Membranes Derived from Sulfonated Hydrocarbon and Inorganic Materials. *J. Power Sources* **2003**, *124*, 18−25.

(12) Wu, J.; Yuan, X. Z.; Martin, J. J.; Wang, H.; Zhang, J.; Shen, J.; Wu, S.; Merida, W. A Review of PEM Fuel Cell Durability: Degradation Mechanisms and Mitigation Strategies. *J. Power Sources* **2008**, *184*, 104−119.

(13) Tseng, C.-Y.; Ye, Y.-S.; Cheng, M.-Y.; Kao, K.-Y.; Shen, W.-C.; Rick, J.; Chen, J.-C.; Hwang, B.-J. Sulfonated Polyimide Proton Exchange Membranes with Graphene Oxide show Improved Proton Conductivity, Methanol Crossover Impedance, and Mechanical Properties. *Adv. Energy Mater.* **2011**, *1*, 1220−1224.

(14) Marani, D.; D'Epifanio, A.; Traversa, E.; Miyayama, M.; Licoccia, S. Titania Nanosheets (TNS)/Sulfonated Poly Ether Ether Ketone (SPEEK) Nanocomposite Proton Exchange Membranes for Fuel Cells. *Chem. Mater.* **2009**, *22*, 1126−1133.

(15) Jung, H.-Y.; Park, J.-K. Long-Term Performance of DMFC Based on the Blend Membrane of Sulfonated Poly(ether ether ketone) and Poly(vinylidene fluoride). *Int. J. Hydrogen Energy* **2009**, *34*, 3915−3921.

(16) Kim, D. H.; Choi, J.; Hong, Y. T.; Kim, S. C. Phase Separation and Morphology Control of Polymer Blend Membranes of Sulfonated and Nonsulfonated Polysulfones for Direct Methanol Fuel Cell Application. *J. Membr. Sci.* **2007**, *299*, 19−27.

(17) Smitha, B.; Sridhar, S.; Khan, A. A. Solid Polymer Electrolyte Membranes for Fuel Cell Applications-A Review. *J. Membr. Sci.* **2005**, *259*, 10−26.

(18) Thanganathan, U.; Dixon, D.; Ghatty, S. L.; Rambabu, B. Development of Non-Perfluorinated Hybrid Materials for Single-Cell Proton Exchange Membrane Fuel Cells. *Int. J. Hydrogen Energy* **2012**, *37*, 17180−17190.

(19) Lee, D.; Song, S. H.; Hwang, J.; Jin, S. H.; Park, K. H.; Kim, B. H.; Hong, S. H.; Jeon, S. Enhanced Mechanical Properties of Epoxy Nanocomposites by Mixing Noncovalently Functionalized Boron Nitride Nanoflakes. *Small* **2013**, *9*, 2602−2610.

(20) Zhi, C.; Bando, Y.; Tang, C.; Kuwahara, H.; Golberg, D. Large-Scale Fabrication of Boron Nitride Nanosheets and Their Utilization in Polymeric Composites with Improved Thermal and Mechanical Properties. *Adv. Mater.* **2009**, *21*, 2889−2893.

(21) Ayrilmis, N.; Dundar, T.; Kaymakci, A.; Ozdemir, F.; Kwon, J. H. Mechanical and Thermal Properties of Wood-Plastic Composites Reinforced with Hexagonal Boron Nitride. *Polym. Compos.* **2014**, *35*, 194−200.

(22) Shi, Y.; Hamsen, C.; Jia, X.; Kim, K. K.; Reina, A.; Hofmann, M.; Hsu, A. L.; Zhang, K.; Li, H.; Juang, Z.-Y.; Dresselhaus, M. S.; Li, L.-J.; Kong, J. Synthesis of Few-Layer Hexagonal Boron Nitride Thin Film by Chemical Vapor Deposition. *Nano Lett.* **2010**, *10*, 4134−4139.

(23) Song, L.; Ci, L.; Lu, H.; Sorokin, P. B.; Jin, C.; Ni, J.; Kvashnin, A. G.; Kvashnin, D. G.; Lou, J.; Yakobson, B. I.; Ajayan, P. M. Large Scale Growth and Characterization of Atomic Hexagonal Boron Nitride Layers. *Nano Lett.* **2010**, *10*, 3209−3215.

(24) Golberg, D.; Bando, Y.; Huang, Y.; Terao, T.; Mitome, M.; Tang, C.; Zhi, C. Boron Nitride Nanotubes and Nanosheets. *ACS Nano* **2010**, *4*, 2979−2993.

(25) Kho, J.-G.; Moon, K.-T.; Kim, J.-H.; Kim, D.-P. Properties of Boron Nitride (BxNy) Films Produced by the Spin-Coating Process of Polyborazine. *J. Am. Ceram. Soc.* **2000**, *83*, 2681−2683.

(26) Zhi, C.; Bando, Y.; Tang, C.; Golberg, D. Boron Nitride Nanotubes. *Mater. Sci. Eng. R* **2010**, *70*, 92−111.

(27) Coleman, J. N.; Lotya, M.; O'Neill, A.; Bergin, S. D.; King, P. J.; Khan, U.; Young, K.; Gaucher, A.; De, S.; Smith, R. J.; Shvets, I. V.; Arora, S. K.; Stanton, G.; Kim, H.-Y.; Lee, K.; Kim, G. T.; Duesberg, G. S.; Hallam, T.; Boland, J. J.; Wang, J. J.; Donegan, J. F.; Grunlan, J. C.; Moriarty, G.; Shmeliov, A.; Nicholls, R. J.; Perkins, J. M.; Grieveson, E. M.; Theuwissen, K.; McComb, D. W.; Nellist, P. D.; Nicolosi, V. Two-Dimensional Nanosheets Produced by Liquid Exfoliation of Layered Materials. *Science* **2011**, *331*, 568−571.

(28) Joly, S.; Garnaud, G.; Ollitrault, R.; Bokobza, L.; Mark, J. E. Organically Modified Layered Silicates as Reinforcing Fillers for Natural Rubber. *Chem. Mater.* **2002**, *14*, 4202−4208.

(29) Bao, C.; Guo, Y.; Song, L.; Kan, Y.; Qian, X.; Hu, Y. In Situ Preparation of Functionalized Graphene Oxide/Epoxy Nanocomposites with Effective Reinforcements. *J. Mater. Chem.* **2011**, *21*, 13290−13298.
(30) Park, S.; Jin, S.; Jun, G.; Jeon, S.; Hong, S. Enhanced Electrical Properties in Carbon Nanotube/Poly (3-hexylthiophene) Nanocomposites Formed Through Non-Covalent Functionalization. *Nano Res.* **2011**, *4*, 1129−1135.
(31) Terao, T.; Zhi, C.; Bando, Y.; Mitome, M.; Tang, C.; Golberg, D. Alignment of Boron Nitride Nanotubes in Polymeric Composite Films for Thermal Conductivity Improvement. *J. Phys. Chem. C* **2010**, *114*, 4340−4344.
(32) Zhi, C.; Bando, Y.; Tang, C.; Honda, S.; Sato, K.; Kuwahara, H.; Golberg, D. Covalent Functionalization: Towards Soluble Multiwalled Boron Nitride Nanotubes. *Angew. Chem., Int. Ed.* **2005**, *44*, 7932−7935.
(33) Zhi, C.; Bando, Y.; Tang, C.; Honda, S.; Sato, K.; Kuwahara, H.; Golberg, D. Characteristics of Boron Nitride Nanotube-Polyaniline Composites. *Angew. Chem., Int. Ed.* **2005**, *44*, 7929−7932.
(34) Zhi, C.; Bando, Y.; Tang, C.; Xie, R.; Sekiguchi, T.; Golberg, D. Perfectly Dissolved Boron Nitride Nanotubes Due to Polymer Wrapping. *J. Am. Chem. Soc.* **2005**, *127*, 15996−15997.
(35) Song, S. H.; Park, K. H.; Kim, B. H.; Choi, Y. W.; Jun, G. H.; Lee, D. J.; Kong, B.-S.; Paik, K.-W.; Jeon, S. Enhanced Thermal Conductivity of Epoxy-Graphene Composites by Using Non-Oxidized Graphene Flakes with Non-Covalent Functionalization. *Adv. Mater.* **2013**, *25*, 732−737.
(36) Shanmugam, M.; Jacobs-Gedrim, R.; Durcan, C.; Yu, B. 2D Layered Insulator Hexagonal Boron Nitride Enabled Surface Passivation in Dye Sensitized Solar Cells. *Nanoscale* **2013**, *5*, 11275−11282.
(37) Yang, G. H.; Shi, J. J.; Wang, S.; Xiong, W. W.; Jiang, L. P.; Burda, C.; Zhu, J. J. Fabrication of a Boron Nitride-Gold Nanocluster Composite and Its Versatile Application for Immunoassays. *Chem. Commun.* **2013**, *49*, 10757−10759.
(38) Huang, X.; Zhi, C.; Jiang, P.; Golberg, D.; Bando, Y.; Tanaka, T. Polyhedral Oligosilsesquioxane-Modified Boron Nitride Nanotube based Epoxy Nanocomposites: An Ideal Dielectric Material with High Thermal Conductivity. *Adv. Funct. Mater.* **2013**, *23*, 1824−1831.
(39) Weng, Q.; Wang, X.; Zhi, C.; Bando, Y.; Golberg, D. Boron Nitride Porous Microbelts for Hydrogen Storage. *ACS Nano* **2013**, *7*, 1558−1565.
(40) Oh, K.-H.; Kim, W.-K.; Sung, K. A.; Choo, M.-J.; Nam, K.-W.; Choi, J. W.; Park, J.-K. A Hydrophobic Blend Binder for Anti-Water Flooding of Cathode Catalyst Layers in Polymer Electrolyte Membrane Fuel Cells. *Int. J. Hydrogen Energy* **2011**, *36*, 13695−13702.
(41) Xu, Y.; Bai, H.; Lu, G.; Li, C.; Shi, G. Flexible Graphene Films via the Filtration of Water-Soluble Noncovalent Functionalized Graphene Sheets. *J. Am. Chem. Soc.* **2008**, *130*, 5856−5857.
(42) Liang, Y.; Wu, D.; Feng, X.; Müllen, K. Dispersion of Graphene Sheets in Organic Solvent Supported by Ionic Interactions. *Adv. Mater.* **2009**, *21*, 1679−1683.
(43) Li, F.; Bao, Y.; Chai, J.; Zhang, Q.; Han, D.; Niu, L. Synthesis and Application of Widely Soluble Graphene Sheets. *Langmuir* **2010**, *26*, 12314−12320.
(44) Chen, Y.; Zhang, X.; Yu, P.; Ma, Y. Stable Dispersions of Graphene and Highly Conducting Graphene Films: A New Approach to Creating Colloids of Graphene Monolayers. *Chem. Commun.* **2009**, 4527−4529.
(45) Rafiee, M. A.; Rafiee, J.; Srivastava, I.; Wang, Z.; Song, H.; Yu, Z.-Z.; Koratkar, N. Fracture and Fatigue in Graphene Nanocomposites. *Small* **2010**, *6*, 179−183.
(46) RamanathanT; Abdala, A. A.; StankovichS; Dikin, D. A.; Herrera Alonso, M.; Piner, R. D.; Adamson, D. H.; Schniepp, H. C.; ChenX; Ruoff, R. S.; Nguyen, S. T.; Aksay, I. A.; Prud'Homme, R. K.; Brinson, L. C. Functionalized Graphene Sheets for Polymer Nanocomposites. *Nat. Nanotechnol.* **2008**, *3*, 327−331.
(47) Yang, S.-Y.; Lin, W.-N.; Huang, Y.-L.; Tien, H.-W.; Wang, J.-Y.; Ma, C.-C. M.; Li, S.-M.; Wang, Y.-S. Synergetic Effects of Graphene Platelets and Carbon Nanotubes on the Mechanical and Thermal Properties of Epoxy Composites. *Carbon* **2011**, *49*, 793−803.
(48) LeBaron, P. C.; Wang, Z.; Pinnavaia, T. J. Polymer-Layered Silicate Nanocomposites: An Overview. *Appl. Clay. Sci.* **1999**, *15*, 11−29.
(49) Tseng, C.-H.; Wang, C.-C.; Chen, C.-Y. Functionalizing Carbon Nanotubes by Plasma Modification for the Preparation of Covalent-Integrated Epoxy Composites. *Chem. Mater.* **2006**, *19*, 308−315.
(50) Kim, Y. S.; Dong, L.; Hickner, M. A.; Glass, T. E.; Webb, V.; McGrath, J. E. State of Water in Disulfonated Poly(arylene ether sulfone) Copolymers and a Perfluorosulfonic Acid Copolymer (Nafion) and Its Effect on Physical and Electrochemical Properties. *Macromolecules* **2003**, *36*, 6281−6285.
(51) Siu, A.; Schmeisser, J.; Holdcroft, S. Effect of Water on the Low Temperature Conductivity of Polymer Electrolytes. *J. Phys. Chem. B* **2006**, *110*, 6072−6080.
(52) Asaka, K.; Fujiwara, N.; Oguro, K.; Onishi, K.; Sewa, S. State of Water and Ionic Conductivity of Solid Polymer Electrolyte Membranes in Relation to Polymer Actuators. *J. Electroanal. Chem.* **2001**, *505*, 24−32.
(53) Borup, R.; Meyers, J.; Pivovar, B.; Kim, Y. S.; Mukundan, R.; Garland, N.; Myers, D.; Wilson, M.; Garzon, F.; Wood, D.; Zelenay, P.; More, K.; Stroh, K.; Zawodzinski, T.; Boncella, J.; McGrath, J. E.; Inaba, M.; Miyatake, K.; Hori, M.; Ota, K.; Ogumi, Z.; Miyata, S.; Nishikata, A.; Siroma, Z.; Uchimoto, Y.; Yasuda, K.; Kimijima, K.-i.; Iwashita, N. Scientific Aspects of Polymer Electrolyte Fuel Cell Durability and Degradation. *Chem. Rev.* **2007**, *107*, 3904−3951.
(54) Springer, T. E.; Zawodzinski, T. A.; Wilson, M. S.; Gottesfeld, S. Characterization of Polymer Electrolyte Fuel Cells Using AC Impedance Spectroscopy. *J. Electrochem. Soc.* **1996**, *143*, 587−599.